LANGMUIR

UNIVERSITY OF Hull

Subscriber access provided by UNIVERSITY OF HULL

Article

Spectrophotometry of thin films of light absorbing particles

Bernard P. Binks, Paul David Ian Fletcher, Andrew J. Johnson, Ioannis Marinopoulos, Jonathan M. Crowther, and Michael A. Thompson

Langmuir, **Just Accepted Manuscript** • DOI: 10.1021/acs.langmuir.6b04443 • Publication Date (Web): 29 Mar 2017

Spectrophotometry of thin films of light absorbing particles

Bernard P. Binks[a], Paul D.I. Fletcher[a]*, Andrew J. Johnson[ad], Ioannis Marinopoulos[a], Jonathan M. Crowther[b] and Michael A. Thompson[c]

[a]*Department of Chemistry, University of Hull, Hull HU6 7RX, UK*
[b]*GSK Consumer Healthcare (UK) Ltd., 980 Great West Road, Brentford, Middlesex, TW8 9GS, UK*
[c]*GSK Consumer Healthcare, 184 Liberty Corner Rd, Warren, NJ, 07059, USA*
[d]*Now at GSK, Harmire Road, Barnard Castle, County Durham, DL12 8DT, UK*

*** Corresponding author**
Prof. Paul D.I. Fletcher
Department of Chemistry,
University of Hull, Hull HU6 7RX, UK
Tel. +44(0)1482 465433
Email P.D.Fletcher@hull.ac.uk

Abstract

Thin films of dispersions of light absorbing solid particles or emulsions containing a light absorbing solute all have a non-uniform distribution of light absorbing species throughout the sample volume. This results in non-uniform light absorption over the illuminated area which causes the optical absorbance, as measured using a conventional specular UV-vis spectrophotometer, to deviate from the Beer-Lambert relationship. We have developed a theoretical model to account for the absorbance properties of such films which are shown to depend on the size and volume fraction of the light absorbing particles plus other sample variables. We have compared model predictions with measured spectra for samples consisting of emulsions containing a dissolved light absorbing solute. Using no adjustable parameters, the model successfully predicts the behaviour of non-uniform, light absorbing emulsion films with varying values of droplet size, volume fraction and other parameters.

Introduction

UV-vis spectrophotometry is very widely used to determine light transmittance through a sample as a function of light wavelength. A conventional spectrophotometer measures the specular transmitted light intensity (I) divided by the incident light intensity (I_o) averaged over the illuminated and detected sample area. At each wavelength, the absorbance (A) is derived according to $A = -\log_{10}(I/I_o)$. In general, the total absorbance results from light transmittance losses due to reflection, scattering and absorption of the incident light. The small absorbance contribution due to transmittance losses caused by light reflection at the front and back faces of the cuvette sample holder is normally determined using a suitable reference cuvette measurement which is then subtracted from the overall absorbance. When corrected for these reflection losses, the reported absorbance of a sample consisting of a molecular solution containing one or more absorbing species which are uniformly distributed throughout the sample volume and which do not scatter light significantly is due solely to light absorption by the dissolved species. This corrected absorbance is related to the sample composition according to the Beer-Lambert relationship

$$A = d \sum_i c_i \varepsilon_i \qquad 1$$

where d is the path length of the light through the sample, c_i is the concentration of the ith absorbing species and ε_i is the wavelength-dependent, molar extinction coefficient of the ith species. Using equation 1, UV-vis spectrophotometry measurements can be used to derive either spectral information (*i.e.* ε_i as a function of wavelength) or solute concentrations. The Beer-Lambert relationship is obeyed with reasonable precision for many different solution systems, *i.e.* ε_i for the absorbing solute is independent of its concentration c_i. In systems where significant deviations do occur (due to processes such as aggregation of the absorbing solutes), concentration-dependent values of ε_i can be measured and used to derive reliable values of solute concentrations.

The main focus of this paper concerns the light transmittance behaviour of thin film samples consisting of light-absorbing particles dispersed in a solvent. Unlike solutions of light absorbing species which are single-phase and contain a uniform distribution of light absorbing species, the distribution of light absorbing species in multi-phase particulate samples is non-uniform which causes the extent of light absorption to vary across the illuminated area. Samples of this type include dispersions of solid organic dyes/pigments, inorganic particles such as semiconductor metal oxides and emulsions containing one or more light absorbing solutes dissolved in either the liquid droplets or continuous phase of the emulsion. Dispersions and/or emulsions containing non-uniformly distributed light absorbing species are widely used in coatings, paints, inks, sunscreens and other applications in which light transmittance properties of thin films are important. For example, sunscreen films are generally applied at film thicknesses in the range 10-20 μm and contain a mixture of UV-absorbing dissolved molecules and small semiconductor metal oxide solid particles contained within either a solution, dispersion or emulsion[1-3]. We note here that, although specular transmittance is important in the range of application areas listed above, many additional factors (*e.g.* reflectance for inks and paints, diffuse transmittance) in addition to the specular component exist for sunscreens *etc*. For the example of sunscreens, the complex effects driven by sunscreen film evaporation on the film optical properties are detailed in refs. 2 and 3. In addition to the application areas listed above, understanding how conventional spectrophotometric measurements of colloidal dispersions of light absorbing species can be related to the concentration could provide a useful tool for the analysis of colloids.

Films containing emulsion drops or solid particles exhibit non-uniform absorption when the emulsion drop or particle size is comparable to the film thickness and do not obey the Beer-Lambert relationship for two main reasons. Firstly, light transmittance loss due to scattering in addition to absorption may be significant. Secondly, the non-uniform distribution of light absorbing species within the sample can cause the measured absorbance to be different to that predicted according to equation 1.

Light transmission through sample films which both scatter and absorb light is complex[4-7]. The interplay between scattering and absorption can give rise to effects including enhancement of dye absorbance by the addition of scattering particles. As discussed later, light transmission losses due to scattering may or may not be recorded as an increase in absorbance when using a specular spectrophotometer. Light scattered at small scattering angles (*i.e*. strongly forward scattering) which is within the spectrophotometer detector acceptance angular range is detected along with the normal transmitted light and thus does not contribute to the reported absorbance. Only light scattered at scattering angles larger than the detector acceptance angular range contributes to the reported absorbance. In addition to scattering effects, film non-uniformity can cause deviations from Beer-Lambert behaviour. Mainly in relation to sunscreen films, there has been extensive literature discussion of how film non-uniformity resulting from point-to-point variation in film thickness can affect the measured optical absorbance of a sample film[8-13]. However, film non-uniformity can also result from non-uniform distribution of light absorbing species within a film of uniform thickness. This is discussed in detail in the Theory section below.

Measuring the (area-averaged) absorbance is one method to characterise sample films in which the light absorbing species are distributed non-uniformly. It is relevant here to note that microscopic methods have been developed to produce pixel-by-pixel visible light absorbance images of lab-on-a chip microreactor channels[14] and biological sporopollenin particles[12]. So far, these microscopic absorbance imaging methods have only been applied at one single wavelength in the visible region of the spectrum.

The main aim of this study is to elucidate how and when the light transmittance properties of films with non-uniform absorption deviate from Beer-Lambert behaviour. This paper is organised as follows. Following the experimental section, a theoretical model is developed to predict how the measured absorbance varies with wavelength for samples of different path length, particle size and volume fraction and light absorption properties. This theoretical model is validated by comparison of model predictions with experimental measurements for thin films of emulsions containing a dissolved light absorbing solute. The experimental emulsion plus solute systems use ingredients commonly found in many sunscreen formulations. Calculated and measured results are compared to show the effects of varying particle size, light absorbing solute concentration, particle volume fraction, emulsion type and the distribution of solute between the droplets and continuous phase of the emulsion. In addition, the behaviour of both strongly and weakly light scattering films is investigated. Finally, the main conclusions are summarised and the wider applicability of the results to non-uniform films other than the emulsion films with applications in sunscreens (as used here) is discussed.

Experimental

Materials

Two different light absorbing solutes found in some commercial sunscreen formulations were used in this work. Their chemical structures are shown in Figure S1 and their extinction coefficient spectra in the different solvents used are shown in Figures S2 and S3. As illustrated in Figure S2, it was checked that solutions of each solute/solvent system obeyed the Beer-Lambert law by measuring absorbance *versus* wavelength for a wide range of different concentrations and path lengths, converting them to extinction coefficient versus wavelength and checking that constant values of extinction coefficient were obtained for all concentrations. Concentration-averaged values of extinction coefficient *versus* wavelength were used for all calculations shown here. 4-*tert*-butyl-4'-methoxy dibenzoyl methane (Avobenzone, abbreviated here as AVB, Sigma-Aldrich, pharmaceutical secondary standard grade) was used as received. Isopentyl *p*-methoxycinnamate (Neo Heliopan E1000, abbreviated here as MC) was kindly donated by the industrial sponsor (GSK) and used as received. Water was purified by reverse osmosis (Elgastat Prima) followed by treatment using a Millipore Milli-Q reagent water system. Squalane (Sigma-Aldrich, 99% purity) was columned over neutral aluminium oxide (Merck) to remove any polar impurities. Propane-1,2-diol (Sigma-Aldrich, > 99%, abbreviated as PG) was used as received. Sucrose (Sigma Aldrich, ≥99.5%), added to match the refractive index (RI) of squalane + aqueous phase emulsions, was used as received. The fumed silica particles used for stabilisation of the emulsions had a specific surface area of 200 m^2 g^{-1} and primary particle diameters of 10–30 nm. They were surface modified by grafting with dichlorodimethylsilane (DCDMS) to obtain particles of different hydrophobicity. Silica particle hydrophobicity is expressed as the % of unmodified surface silanol groups present after modification (where 100% SiOH corresponds to maximally hydrophilic and lower % SiOH corresponds to increasing hydrophobicity). Silica particles with % SiOH ranging from 14-100% were provided by Wacker-Chemie (Germany) and used as received.

Methods

UV/Vis spectra were measured using a double beam Unicam UV3 spectrophotometer. Samples were contained in quartz cuvettes (Hellma Analytics) of path lengths ranging from 0.001 to 1 cm which were mounted horizontally within the spectrophotometer, *i.e.* the incident light path was vertical through the cuvette plus sample. This sample orientation prevented gravity-driven sedimentation or creaming along the long axis of the cuvette but sedimentation/creaming parallel to the light path was still possible. Effects due to creaming or sedimentation were minimised by strongly shaking the samples immediately prior to recording their spectra. The spectrophotometer used measures the *specular* optical transmittance (with subsequent conversion to absorbance) with a detector acceptance angle estimated to be $<5^o$ either side of normal incidence (but not known precisely). Transmitted light emerging from the sample at angles greater than the detector acceptance angle (*e.g.* light scattered at scattering angles greater than a few degrees) is not detected and therefore contributes to the apparent absorbance measured by this instrument. In use, this double-beam instrument was first zeroed with air in both sample and reference beams. Spectra of solution or emulsion samples containing a light absorbing solute were measured with air in the reference beam. Reference spectra of the solvent or emulsion sample without the dissolved light absorbing solute *versus* air were separately measured. Spectra of the solute alone were obtained by subtraction of the reference spectrum from the sample spectrum. Using repeated measurements, it was found that peak absorbance values of solution samples were reproducible within 2%. Probably because of the variability in the extent of sedimentation or

creaming, the reproducibility of emulsion samples was worse; peak absorbance values had an uncertainty of approximately 8%.

Silica particle-stabilised emulsions were prepared as follows. The masses of the two liquids (containing the required dissolved solutes) and the stabilising silica particle powder (with the appropriate % SiOH) required to produce approximately 10 cm^3 of emulsion were added to glass vessels of 28 mm diameter by 72 mm height. Each mixture was emulsified using an IKA Ultra–Turrax T25 homogeniser with a rotor-stator head of 18 mm diameter operating at 13,000 rpm for 2 minutes at room temperature (21^{o}C). The emulsion type was determined shortly after preparation by observing whether a drop of the prepared emulsion dispersed or not when added to either pure solvent of the emulsion. The emulsion drop is observed to disperse only in the solvent which forms the continuous phase of the emulsion. For particle-stabilised emulsions containing equal volumes of the two liquids, the emulsion type is controlled by the wettabilities of the stabilising particles by the two solvents of the emulsion[15]. Thus, silica particles of different % SiOH were used to obtain the different emulsion types used in this work. As discussed in ref. 15, the mean droplet size in the emulsion is dependent on the concentration of the stabilising particles; high particle concentration gives small droplets and low concentrations produce large droplets. Thus, emulsions with different droplet sizes were produced by using different silica particle concentrations in the range 1 – 5 wt.%. Optically transparent squalane-in-water+sucrose and water+sucrose-in-squalane emulsions were produced by adding sucrose to the aqueous phase to increase its refractive index (RI) value from 1.333 (pure water) to the value for squalane (1.445, value from ref. 16). The RI-matching condition was obtained by addition of 63.5 wt.% sucrose to the aqueous phase. Optical micrographs of the non-RI matched emulsions were obtained using an Olympus BX51 microscope equipped with an Olympus DP70 camera and ImageJ software and operating in transmission mode. For the optically transparent RI-matched emulsion samples, approximately 1 x 10^{-7} M fluorescein was added to the aqueous phases of the emulsions. The Olympus BX51 microscope operating in fluorescence microscopy mode with the appropriate filter set was then used to image the emulsions. Emulsion drop size distributions were obtained from the microscope images by analysis of not less than 50 drops on each image. All emulsions were observed to be very stable with respect to droplet coalescence. Examples of the % SiOH and silica particle concentrations used to obtain the different emulsion types and mean droplet sizes used in this work are summarised in Table 1. It can be seen that emulsions in which the polar liquid forms the continuous phase require more hydrophilic silica particles (*i.e.* larger values of % SiOH) than the inverse emulsion type. Droplet size polydispersities (expressed as the distribution standard deviation divided by the mean) are around 20% for all the different emulsion systems.

Results and Discussion

Theory

As discussed in the Introduction, a conventional spectrophotometer measures the specular light transmittance (equal to the transmitted light intensity I divided by the incident light intensity I_o) averaged over the illuminated and detected sample area. The derived absorbance A for solution samples which are non-scattering and contain a uniform distribution of light absorbing species obey the Beer-Lambert relationship (equation 1). Samples which consist of light absorbing particles dispersed in a continuous phase do not, in general, obey the Beer-Lambert relationship for two main reasons. Firstly, they generally

scatter light significantly in addition to absorbing it. Secondly, when the particle radius r is comparable with the path length (*i.e.* within the approximate range $d > 2r > d/10$), the distribution of light absorbing material over the illuminated area of the sample will be significantly non-uniform. This has the result that the light transmittance through the sample will vary from point to point within the illuminated area. This situation is shown schematically in Figure 1.

We seek to develop a model to account for how the measured specular absorbance of thin films containing a non-uniform distribution of absorbing species varies with absorbing particle size, the absorption properties of the particle material, the path length and other variables. We first consider the effects of light scattering by the particles. In many relevant practical systems such as coatings and sunscreens, the film thickness (equal to the optical path length) is of the order of tens of μm and hence the particle sizes relevant to the model developed here are typically greater than 1 μm. These particle sizes, including the emulsion droplets in the experimental systems used here, are large relative to the wavelength range of the UV-Vis incident light and Mie theory can be used to calculate their scattering properties. Using MiePlot software available on the internet[17], we have calculated the scattering efficiency (equal to the effective scattering cross section divided by the geometrical cross sectional area of the scattering particle) *versus* wavelength for squalane droplets in water for radii from 5 to 50 μm with polydispersities (standard deviation/mean) of 20%. Using equation S1 (derived as shown from equation 6 in ref. 5), the calculated scattering efficiencies were converted to the absorbance contribution due to scattering (A_{scat}). As seen in Figure S4, A_{scat} is almost independent of wavelength and increases with decreasing droplet size for this system. Figure S4 also shows plots of the normalised scattering intensity versus scattering angle calculated for the mid-range wavelength of 300 nm (again calculated using MiePlot software[17]). The emulsion droplets scatter light strongly in the forward direction, *i.e.* at small scattering angles. The scattering intensity shifts to smaller scattering angles for larger droplet sizes. The calculations for 20 μm droplets in Figure S4 can be compared with the measured specular absorbance of the same emulsion (with no added light absorbing solute) shown in Figure S5. Similar to the calculated plot, the measured specular absorbance due to scattering is only weakly dependent on wavelength. The average measured value of A_{scat} (approximately 1 absorbance unit) is less than the calculated value of 1.65 absorbance units. Specular spectrophotometers detect light transmitted only over an angular range of less than a few degrees from the direction of the incident light. Thus, only light scattered at scattering angles greater than the detector acceptance angular range contributes to the measured, apparent absorbance due to scattering. This is the reason why the measured (specular) value of A_{scat} is less than the calculated value. In confirmation of this interpretation, the value of A_{scat} for similar emulsion systems has been shown to reduce to zero when measured using a *diffuse* transmittance spectrophotometer with a detector acceptance angle of 60^{o} [3]. Overall, the calculations reveal that the scattering contribution to the measured absorbance spectrum of a thin film of particles consists of an approximately constant absorbance (*i.e.* only weakly wavelength dependent) which corresponds to the fraction of scattered light which falls outside the detector acceptance range.

For large particles scattering light only at small forward angles, the scattered light path is not significantly different to the overall sample cuvette path length experienced by non-scattered photons. In this situation, when samples both absorb and scatter light, the absorbance contribution due to light absorption is not affected by alteration of the "effective" light path length due to scattering. In principle, strong multiple scattering could increase the apparent absorbance due to light absorption by a light-absorbing solute by increasing the

"effective" path length of the multiply scattered light. This effect has been demonstrated by addition of strongly scattering particles to a light absorbing solution but is significant only when the absorbance due to scattering is more than 3 times larger than the absorbance due to absorption[7]. This is not the case for the experimental systems used here and so this effect is assumed to be negligible.

Based on the considerations discussed above, we take the measured absorbance (corrected for light reflection losses) to be the sum of the contributions from scattering (A_{scat}) and absorption (A_{abs}). Figures S5 and S6 show examples of measured spectra of emulsion films with and without light absorbing solute. Subtraction of the reference spectrum from the sample spectrum yields the spectrum due solely to the light absorbing solute, *i.e.* A_{abs} versus wavelength. Figure S5 shows an example of a non-RI-matched (*i.e.* relatively strongly scattering) emulsion film for which the contributions A_{scat} and A_{abs} are similar in magnitude in the wavelength range where the solute absorbs. Figure S6 shows the contribution of A_{scat} to the overall absorbance for an RI-matched (*i.e.* weakly scattering) emulsion film is negligibly small.

We next consider how the absorption contribution A_{abs} can be modelled. We consider a sample consisting of a dispersion of monodisperse spherical particles of radius r positioned randomly throughout a horizontal thin film of depth equal to the optical path length d. As shown schematically in Figure 1, light entering the sample at different points can pass through either 0, 1, 2, 3,…. individual particles before exiting the cuvette and thus the light transmittance will vary from point to point. The measured absorbance is derived from the overall transmittance averaged over the illuminated area. The total sample depth d is divided into an integral number (N_{layer}) of horizontal layers which are indicated by the horizontal dashed lines in Figure 1. We take N_{layer} to be equal to d/2r and round up N_{layer} to the nearest integer if d/2r is non-integral. Rather than consider the complex problem of spherical particles in different layers overlapping, we simplify calculations by modelling the spherical particles as equivalent cylinders of length = d/N_{layer} and radius r_c, as indicated in Figure 1. The equivalent cylinders are aligned parallel to the light path and have the same volume as the spherical particles. Hence:

$$\frac{4\pi r^3}{3} = \frac{d\pi r_c^2}{N_{layer}} \qquad \text{and so} \qquad r_c^2 = \frac{4r^3 N_{layer}}{3d} \qquad 2$$

Within each of these layers, the number of particles per unit layer area n_{layer} is

$$n_{layer} = \frac{3\phi d}{4\pi r^3 N_{layer}} \qquad 3$$

where ϕ is the volume fraction of particles in the sample. The area fraction occupied by the equivalent cylindrical particles in each layer f_{layer} is equal to the product of the number of particles per unit area in the layer multiplied by the projected area of one cylindrical particle. Substitution for r_c^2 from equation 2 into the resultant equation gives the final result for f_{layer}.

$$f_{layer} = \frac{3\phi d\pi r_c^2}{4\pi r^3 N_{layer}} = \frac{3\phi d\pi}{4\pi r^3 N_{layer}} \frac{4r^3 N_{layer}}{3d} = \phi \qquad 4$$

At each position within the illuminated sample area, the probability P(n) that there are n particles overlapping throughout the sample depth is given by[18]

$$P(n) = \frac{N_{layer}!}{n!(N_{layer}-n)!} f_{layer}^{n}\left(1 - f_{layer}\right)^{(N_{layer}-n)} \quad 5$$

The probability P(n) that the incident light passes through n overlapping particles is equal to the sample area fraction containing n overlapping particles within the total sample depth d. At this point, the incident light experiences a path length through the overlapping particles equal to $d_p(n) = nd/N_{layer}$ and a path length through the continuous phase $d_c(n) = d - d_p(n)$. The measured sample absorbance due to absorption A_{abs}, equal to the negative logarithm of the area weighted transmittance, is then given by:

$$A_{abs} = -log_{10} \sum_{0}^{N_{layer}} P(n)\, 10^{-(d_p(n)\varepsilon_p C_p + d_c(n)\varepsilon_c C_c)} \quad 6$$

where ε_p and ε_c are the extinction coefficients of the absorbing solute in the particle and continuous phases respectively, and C_p and C_c are the solute concentrations in those phases. We note here that equation 6 uses the Beer-Lambert law to derive the absorbances in each different sub-fraction of the illuminated area despite the fact that it is not valid for the overall measured sample absorbance A_{abs}.

Equation 6 is approximate for several reasons. Firstly, the derivation assumes that the spherical particles are monodisperse. Secondly, it is assumed that the particles are positioned randomly throughout the continuous phase volume of the sample (*i.e*. the particles are distributed randomly except that the particle volumes do not overlap). This assumption corresponds to the particles behaving as hard spheres with no additional attractive or repulsive interactions and is likely to become invalid at high particle volume fractions. Dispersions of hard spheres exhibit a liquid + crystal coexistence region for $0.494 < \phi < 0.545$[19] and form a hexagonally close packed system at $\phi = 0.74$. Hence, random distribution of the solid particles is only possible for $\phi < 0.494$. Dispersion of liquid emulsion drops form high internal phase emulsions which have a biliquid foam structure at volume fractions greater than about 0.7[20]. Even at volume fractions lower than these limits, real dispersions of either solid or liquid particles may have non-random distributions because of particle-particle interactions or because the particles sediment or cream to some extent. For the experiments discussed here, the samples are held horizontally within the spectrophotometer and so particle sedimentation/creaming can only occur in the direction parallel to the incident light. This possible effect was minimised by agitating the samples immediately prior to measurement. Thirdly, it is assumed here that the real situation of spherical particles in different layers overlapping can be reasonably well approximated as overlapping equivalent cylindrical particles. Lastly, it is assumed here that the integral number of layers in the total sample depth N_{layer} is obtained by rounding *up* the value of d/2r to the nearest integer whereas we could choose to round the value *down*. The validity of these assumptions and approximations are tested *a posteriori* by comparison with experiment as described below.

In general, for dispersions of absorbing particles which may be either solid particles or emulsion droplets, light absorption may occur in both the particles and the continuous phase. In the case of solid particles of a light absorbing species, the continuous phase will contain a concentration of the light absorbing species equal to the solubility of the species in the continuous phase. In the case of an emulsion containing a dissolved light absorbing species (as used in the experiments described here), the concentration of the species in the droplets and continuous phase will be determined by the species' distribution coefficient

between the two solvents of the emulsion. We define the equilibrium distribution coefficient D to be equal to the ratio of the species concentration in the droplet phase C_d divided by the concentration in the continuous phase C_c

$$D = \frac{C_d}{C_c} \quad (7)$$

The overall species concentration C in the total emulsion volume (known from the emulsion composition) is given by

$$C = \phi C_d + (1 - \phi) C_c \quad (8)$$

Hence, if D is determined, C_d and C_c can be derived using

$$C_c = \frac{C}{(\phi D + 1 - \phi)} \quad \text{and} \quad C_d = DC_c \quad (9)$$

Input data for the model developed here requires the measurement of the extinction coefficient spectra of the absorbing solute in the two solvents of the emulsions (ε_d and ε_c *versus* wavelength, see Figures S2 and S3), the solute distribution coefficient D and the mean emulsion drop radius r. Input of these data together with the path length, overall solute concentration C and droplet volume fraction ϕ into the model represented by equations 2-9 enables prediction of A_{abs} *versus* wavelength *with no adjustable parameters*. Model predictions of A_{abs} can be directly compared with A_{abs} spectra derived from measured overall absorbance spectra by subtraction of the scattering contribution as shown in Figures S5 and S6.

Comparison of theory and experimental data

The experimental systems investigated here consist of nanoparticle-stabilised emulsions which contain a dissolved light absorbing solute. In order to comprehensively test the model discussed above, several types of emulsion system have been studied. The first types, squalane-in-water or water-in-squalane emulsions containing the absorbing solute MC, scatter light and the MC solute partitions exclusively to the squalane phase forming either the droplets or the continuous phase. For these systems, we have measured the effects of varying droplet size, MC concentration, droplet volume fraction and emulsion type with all other parameters fixed and compare the results with model calculations. Secondly, we use weakly-scattering RI-matched emulsions containing MC to test whether the level of scattering affects the model validity. Lastly we use squalane-in-PG and PG-in-squalane emulsions containing either MC or AVB as light absorbing solute. Unlike MC in squalane+water emulsions, these solutes show comparable concentrations in the two liquid phases of the squalane+PG emulsions. Use of these different solute and emulsion systems enables effects due to light scattering, emulsion type and different extents of solute partitioning to be investigated.

We first discuss the behaviour of MC in squalane-in-water emulsions. The solubility of MC in squalane is high (1300 mM) but very low in water (0.15 mM)[3]. The equilibrium partition coefficient between squalane and water is approximately equal to the ratio of MC solubilities in the two solvents and so is estimated to be approximately 9000, *i.e.* the MC is located virtually exclusively in the squalane phase of the emulsions. Figure 2 shows the appearance of a typical emulsion sample contained within a 100 μm path length cuvette and

viewed from the top. It can be seen that the droplets appear to be fairly randomly positioned across the imaged area and throughout the sample depth. The measured specular absorbance spectra of an emulsion sample with and without MC is shown in Figure S5 which also shows the derived A_{abs} spectrum due solely to light absorption by MC. Figure 3 compares the measured and predicted MC spectra in squalane-in-water emulsions of varying droplet size but with all other parameters held constant. The spectra in the non-uniform emulsions are compared with the spectrum expected for a uniform film which is shown as the dashed lines labelled "homogeneous" in the legend (upper plot). It can be seen that the effect of increasing the squalane droplet radius is to progressively decrease the size of the MC absorbance peak (around 300 nm) below that expected for a uniform film of the same overall composition. In addition, the peaks are "flattened" in shape since higher absorbance values are reduced more than small absorbance values. Both these features are successfully predicted by the model calculations (middle plot).

As detailed above, the model represented by equations 2-9 involves dividing the sample depth into an integral number of layers (N_{layer}) and approximates the spherical particles as equivalent volume cylinders. The resulting model calculations predict identical spectra for the range of particle sizes which correspond to the same value of N_{layer}. This effect can be seen in the predicted spectra of the middle plot of Figure 3 (where the legend for each individual spectrum refers to a range of emulsion drop radii) but is most clearly revealed in the lower plot. The lower plot compares measured and calculated values of the peak absorbance at 292 nm. In order to test the choice of rounding up N_{layer} to the nearest integer, we show calculations corresponding to either rounding up or rounding down N_{layer} (corresponding to the solid and dashed lines in the lower plot). It can be seen that measured absorbance values mostly lie between the two calculated lines but that the rounding up choice shows slightly better agreement with the measured values.

Figure 4 shows the effect of varying the MC concentration in squalane-in-water emulsion films whilst holding all other parameters constant. Because the overall MC concentration is changing in this series, the absorbance spectra have been converted to apparent extinction coefficient spectra to enable a more valid comparison. Increasing the MC concentration (*i.e*. making the emulsion droplets more light absorbing) causes a progressive reduction in the extinction coefficient peaks below those expected for a homogeneous film obeying the Beer-Lambert relationship. The measured effects of peak reduction flattening with increasing MC concentration are reasonably well captured by the model calculations. The changes in the apparent extinction coefficient highlight how the Beer-Lambert relationship is not obeyed for the emulsion samples.

Figure 5 compares measured (upper plot) and predicted (middle plot) absorbance spectra for a series of squalane-in-water emulsions containing a constant concentration of MC in the squalane droplets which were diluted with water to obtain different ϕ values whilst maintaining the droplet size. The absorbance peaks decrease with dilution due to the combined effected of decreasing ϕ and $[MC]_{ov}$ as shown in the key. As seen in the lower plot, measured peak absorbance values as a function of ϕ are reasonably well predicted.

As discussed in the theory section above, it is argued that the scattering contribution to the overall absorbance of these emulsion films can be simply subtracted to obtain the absorbance due to light absorption. As shown in Figures 3-5, the absorbance spectra due to light absorption derived in this way for scattering squalane-in-water emulsion films are successfully modelled. In order to further test the effects of the film scattering, we have

compared measured and modelled spectra for emulsions in which the refractive index (RI) of the droplets and continuous phase are matched by addition of sucrose to the water phase. As seen in Figure S6, the absorbance due to scattering of these emulsions is very small. It is worth noting here that the addition of sucrose matches the real parts of the complex RI values of squalane and the aqueous phase. However, the addition of the light absorbing solute (MC in this case) increases the imaginary part of the squalane RI (corresponding to light absorption). Thus, at wavelengths at which the solute absorbs light, the overall, complex RI values are not fully matched and hence some scattering is expected at these wavelengths. Despite this complication, the scattering of the RI-matched systems will be much less than for the non-RI-matched emulsions; hence comparison of measured and predicted absorption spectra in both types of emulsion is expected to reveal whether or not scattering has significant effects which are not accounted for in the model. Figure 6 compares measured and calculated absorption spectra of MC in squalane-in-water+sucrose emulsion samples with different droplet sizes and optical path lengths. As for the non-RI-matched systems, the model correctly predicts the variation in the main peak (around 300 nm) height and shape with both droplet size and the sample path length. However, it can be seen that the measured spectra show some wavelength regions in which the measured absorbance values are larger than the homogeneous case; this behaviour is not predicted by the model. For the low wavelength range (less than 250 nm), this behaviour might possibly be caused by irreproducibility due to minor impurities which are highly absorbing at low wavelengths. However, minor deviations are also observed at wavelengths above 340 nm which are presently unexplained. Overall, we conclude that the behaviour of the main absorbance peak is well described by the model calculations for both weakly scattering (RI-matched) and strongly scattering (non-RI-matched) emulsions discussed earlier.

Finally, we consider the effects of switching the emulsion type and the distribution coefficient of the light absorbing solute on the absorption spectra. We first show model calculations to illustrate the effects of changing the solute distribution coefficient for the case of PG-in-squalane emulsions containing MC as solute. The extinction coefficient spectra of MC in PG and squalane are shown in Figure S3 where it can be seen that the MC absorption shifts to slightly higher wavelengths in PG as compared with squalane as solvent. Although the actual value of D for the distribution of MC between the PG droplets and squalane continuous phase of the emulsions is fixed (see later), we use a range of hypothetical D values in model calculations to illustrate all possible behaviours. Figure 7 shows the calculated MC absorption spectra for different (hypothetical) D values and emulsion droplet volume fractions. When D = 1, the MC solute distribution is uniform throughout the emulsion but the spectral peak shapes change slightly with droplet volume fraction because the MC spectra in the two solvents are slightly different. Relative to the uniform solute distribution case, large absorbance reductions are predicted when *either* $D \gg 1$ and ϕ is small *or* $D \ll 1$ and ϕ is big. Similar calculations for MC in squalane-in-PG emulsions are shown in Figure S7 where it can be seen that the behaviour is similar except that the absorbance peak shape changes originating from the MC spectral differences in the two solvents are reversed.

Comparison of Figures 7 and S7 show the predicted effects of changing the emulsion type when all other parameters are held constant. For this comparison it should be remembered that we have chosen to define the distribution coefficient D as the equilibrium solute concentration in the droplet phase divided by that in the continuous phase (rather than the ratio of the equilibrium concentrations in the two solvents). For this reason the spectrum of MC in a PG-in-squalane emulsion with value D should be compared with the spectrum

with value 1/D in the squalane-in-PG emulsion to see the effect of changing only the emulsion type. Noting this point, it can be seen that changing emulsion type is predicted to show no change in the spectrum for emulsions with $\phi = 0.5$. For other values of ϕ, the spectral changes between the two emulsion types are predicted to be large when either $D >> 1$ or $D << 1$. These situations correspond to the largest non-uniformity of solute distribution in the emulsions.

We have used three different experimental systems to measure the effects of emulsion type and solute distribution coefficient on the solute absorption spectrum. For each solute/emulsion system, the droplet volume fraction ϕ was kept constant at 0.5, the path length was 0.01 cm and the drop size and solute concentration was kept constant for both emulsion types. The first system consisted of MC in squalane-in-water and water-in-squalane emulsions. MC is approximately 9000 times more soluble in squalane than in water and so the values of D are approximately 9000 for squalane-in-water and 1/9000 for water-in-squalane emulsions. Because $\phi = 0.5$, the absorption spectrum is predicted to be identical in the two emulsion types (as for all three systems measured here). Because $D >> 1$ or $D << 1$ (depending on the emulsion type), the solute absorption peak absorbance is predicted to be approximately half the value corresponding to a homogeneous solute distribution. As seen in the upper plot of Figure 8, the measured and calculated spectra are in good agreement. The second system consisted of the solute AVB in squalane-in-PG and PG-in-squalane emulsions. The solubilities of AVB in squalane and PG are 38 and 14 mM respectively[3] and so D is estimated to be approximately 2.7 or 1/2.7 in the two emulsion types. This value of D has been confirmed from photochemical studies[21]. Because D is relatively close to 1, the spectral peaks are predicted to be only slightly reduced relative to the homogeneous case. As seen in the middle plot of Figure 8, measured and calculated peak absorbance values agree within the estimated uncertainty of 5-10%. The third system consisted of MC in squalane-in-PG and PG-in-squalane emulsions for which D = 1.5 or 1/1.5[21]. Because D is again close to 1, this system is expected to show similar behaviour to the AVB system; this expectation is confirmed in the lower plot of Figure 8. Additionally, we have measured the spectra of MC dissolved in RI-matched squalane-in-water+sucrose and water+sucrose-in-squalane emulsions in which the MC partitions strongly to the squalane phase. This system (not shown here) is predicted and measured to behave similarly to the system in the upper plot of Figure 8. Overall, it is concluded that the model correctly predicts the variation of absorption spectra with emulsion type for emulsions containing solutes which partition either strongly or weakly between the emulsion liquid phases.

Conclusions

We have developed a model which, using no adjustable input parameters, successfully predicts the absorbance spectra measured using a specular UV-Vis spectrophotometer of thin film particle dispersion samples with non-uniform light adsorption across the illuminated area. The model has been validated by comparison with experimental measurements of the spectra of thin emulsion films containing a light absorbing solute. Effects of changing particle size, light absorption by the particles, particle volume fraction, optical path length, sample light scattering intensity, switching the light absorbing particles and continuous phase and altering the solute distribution between particles and continuous phase have all been investigated and shown to agree with model predictions within the experimental uncertainty of approximately 10%. The model accounts for how and when measured absorbance values for samples containing a non-uniform distribution of light absorbing species deviate from the Beer-Lambert relationship.

Although emulsion films have been used in the experimental part of this study, the model represented by the schematic diagram of Figure 1 and equations 2-9 is expected to be equally valid for dispersions of solid particles which absorb light such as solid organic dyes or pigments and inorganic particles such as semiconductor metal oxides. Thin films of particle dispersions and/or emulsions are widely used in coatings, paints, inks, sunscreens, cosmetics and other applications in which light transmittance (and other) properties are important. In this study we have shown how deviations from the Beer-Lambert relationship occur for light absorbing particles with radii greater than about 5 μm when in sample films of thickness d = 100 μm. It is important to note that film non-uniformity resulting in deviations from Beer-Lambert behaviour will occur for any r values greater than approximately d/10. Because the film non-uniformity is determined by particle size *relative to the film thickness*, the model is therefore expected to be applicable to a wide range of particle sizes in films of different thicknesses. The lower limit for this range of applicability is expected to be non-uniform films with feature sizes of the order of the wavelength of the illuminating light. For non-uniform films with nm scale features, optical field coupling can occur over the features giving rise to effects which can be engineered to optimise the efficiency of, for example, photovoltaic devices (see, for example, ref. 22 for discussion of these types of system). Finally, we note that the model developed here could be applicable to the inverse problem. Instead of measuring the extinction coefficient spectrum of the light absorbing particle material and predicting the specular absorption spectrum of a dispersion (as done here), one could measure the specular absorption spectrum of a dispersion and use the model to derive the true, intrinsic extinction coefficient spectrum of the particle material.

Acknowledgements

We thank GlaxoSmithKline Consumer Healthcare for funding this work and supplying the samples of UV filters used here.

References

1. Diffey, B. Sunscreen isn't enough. *J. Photochem. Photobiol. B*, **2001**, *64*, 105-108.
2. Binks, B.P.; Brown, J.; Fletcher, P.D.I.; Johnson, A.J.; Marinopoulos, I.; Crowther, J.M.; Thompson, M.A. Evaporation of sunscreen films: how the UV protection properties change. *ACS App. Mater. & Interfaces*, **2016**, *8*, 13270-13281.
3. Binks, B.P.; Fletcher, P.D.I.; Johnson, A.J.; Marinopoulos, I.; Crowther, J.M.; Thompson, M.A. Evaporation of particle-stabilised emulsion sunscreen films. *ACS App. Mater. & Interfaces*, **2016**, *8*, 21201-21213.
4. Bohren, C.F.; Huffman, D.R. *Absorption and Scattering of Light by Small Particles.* Wiley-VCH, Weinheim, **2004**.
5. McClements, D.J. Theoretical Prediction of Emulsion Color. *Adv. Colloid Interface Sci.*, **2002**, *97*, 63-89.
6. Bressel, L.; Reich, O. Theoretical and experimental study of the diffuse transmission of light through highly concentrated absorbing and scattering materials. Part 1: Monte-Carlo simulations. *J. Quantit. Spec. & Radiat. Transfer*, **2014**, *146*, 190-198.
7. Herzog, B.; Sengün, F. Scattering particles increase absorbance of dyes - a model study with relevance for sunscreens. *Photochem. Photobiol. Sci.*, **2015**, *14*, 2054-2063.
8. O'Neill, J.J. Effect of film irregularities on sunscreen efficacy. *J. Pharm. Sci*., **1984**, *73*, 888-891.

9. Ferrero, L.; Pissavini, M.; Marguerie, S.; Zastrow, L. Efficiency of a continuous height distribution model of sunscreen film geometry to predict a realistic sun protection factor. *J. Cosmet. Sci*., **2003**, *54*, 463-481.
10. Herzog, B.; Mongiat, S.; Quass, K.; Deshayes, C. Prediction of sun protection factors and UVA parameters of sunscreens by using a calibrated step film model. *J. Pharm. Sci*., **2004**, *93*, 1780-1795.
11. Ferrero, L.; Pissavini, M.; Doucet, O. How a calculated model of sunscreen film geometry can explain *in vitro* and *in vivo* SPF variation. *Photochem. Photobiol. Sci*., **2010**, *9*, 540-551.
12. Atkin, S.L.; Barrier, S.; Cui, Z-G.; Fletcher, P.D.I.; Mackenzie, G.; Panel, V.; Sol, V.; Zhang, X. UV and visible light screening by individual sporopollenin exines derived from Lycopodium clavatum (club moss) and Ambrosia trifida (giant ragweed). *J. Photochem. Photobiol. B*, **2011**, *102*, 209-217.
13. Herzog, B.; Osterwalder, U. Simulation of sunscreen performance. *Pure & Appl. Chem.*, **2015**, *87*, 937-951.
14. Broadwell, I.; Fletcher, P.D.I.; Haswell, S.J.; McCreedy, T.; Zhang, X. Quantitative 3-dimensional profiling of channel networkswithin transparent 'lab-on-a-chip' microreactors using a digital imaging method. *Lab on a Chip*, **2001**, *1*, 66-71.
15. Chevalier, Y.; Bolzinger, M-A. Emulsions stabilized with solid nanoparticles: Pickering emulsions. *Colloids & Surfaces A*,: **2013**, *439*, 23–34.
16. Dubey, G.P.; Tripathi, N.; Bhatia, S.C. Refractive index of ternary liquid systems of squalane (+ hexane + benzene; + cyclohexane + benzene and + hexane + cyclohexane). *Ind. J. Pure & Appl. Phys.*, **2005**, *43*, 175-179.
17. MiePlot version 4.5.01 downloaded from http://www.philiplaven.com/mieplot.htm
18. Gut, A. *Probability: A Graduate Course*. 2nd edition. Springer, New York, 2013.
19. Cheng, Z.; Chaikin, P.M.; Russel, W.B.; Meyer, W.V.; Zhu, J.; Rogers, R.B.; Ottewill, R.H. Phase diagram of hard spheres. *Mater. Design*, **2001**, *22*, 529-534.
20. Lissant, K.J. The geometry of high-internal-phase-ratio emulsions. *J. Colloid Interface Sci.*, **1996**, *22*, 462-468.
21. Binks, B.P.; Fletcher, P.D.I.; Johnson, A.J.; Marinopoulos, I.; Crowther, J.M.; Thompson, M.A. How the sun protection factor (SPF) of sunscreen films change during solar irradiation. *J. Photochem. Photobiol. A*, **2017**, *333*, 186-199.
22. Tang, Z.; Tress, W.; Inganas, O. Light trapping in thin film organic solar cells. *Mater. Today*, **2014**, 17, 389-396.

Table 1. Examples of the compositions, mean droplet radii and polydispersities for the different emulsion types used in this work. All values listed here refer to emulsions with droplet volume fraction $\phi = 0.5$. Other values of ϕ were obtained by emulsion dilution with the continuous phase.

Emulsion type	%SiOH	Silica particle conc./wt%	Mean droplet radius/μm	Polydispersity (standard deviation)/μm
squalane-in-water	88	5	7.3	2.1
squalane-in-water	88	2	20.7	3.6
squalane-in-water	88	1	41.4	5.1
water-in-squalane	51	1	7.5	2.4
squalane-in-PG	35	1	10	2
PG-in-squalane	23	1	10	2
squalane-in-(water+sucrose)	61	2	4	1
(water+sucrose)-in-squalane	51	2	4	1

Figure 1. Schematic view (perpendicular to the incident light) of a cuvette containing randomly positioned, light absorbing spherical particles (left hand diagram) and the equivalent system used in the theoretical modelling (right hand diagram).

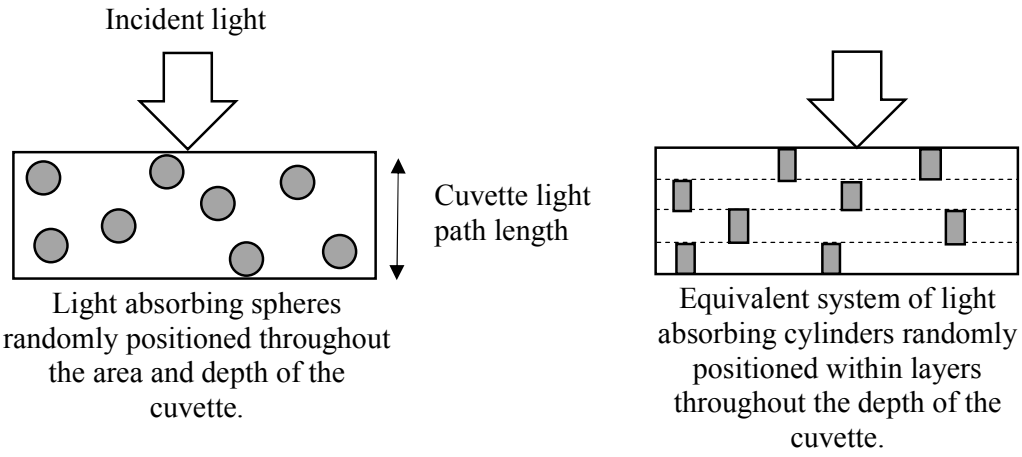

Figure 2. Optical micrograph of a squalane-in-water emulsion stabilised by 1 wt% of 88 %SiOH silica particles with $\phi = 0.5$ within a cuvette of path length = 100 μm. The scale bar = 200 μm and the mean drop diameter = 44 μm with a standard deviation of 7 μm.

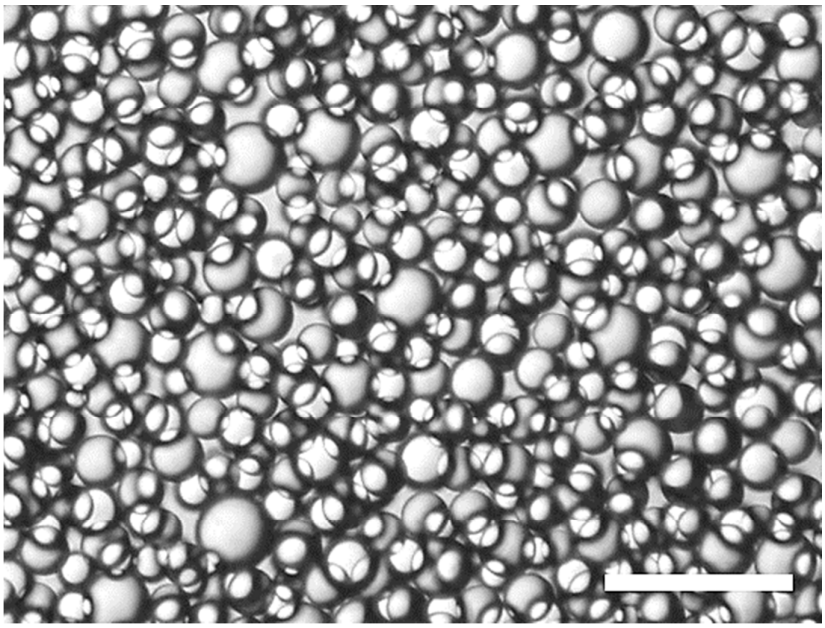

Figure 3. Comparison of measured (upper plot) and calculated (middle plot) absorbance spectra (with the "empty" emulsion as reference) for 100 μm path length of squalane-in-water emulsions with $\phi = 0.5$, $[MC]_{ov} = 10.5$ mM and varying mean drop radii (shown in legend). The lower plot compares the measured absorbances at 292 nm versus drop radius with those calculated with N_{layer} either rounded up or down.

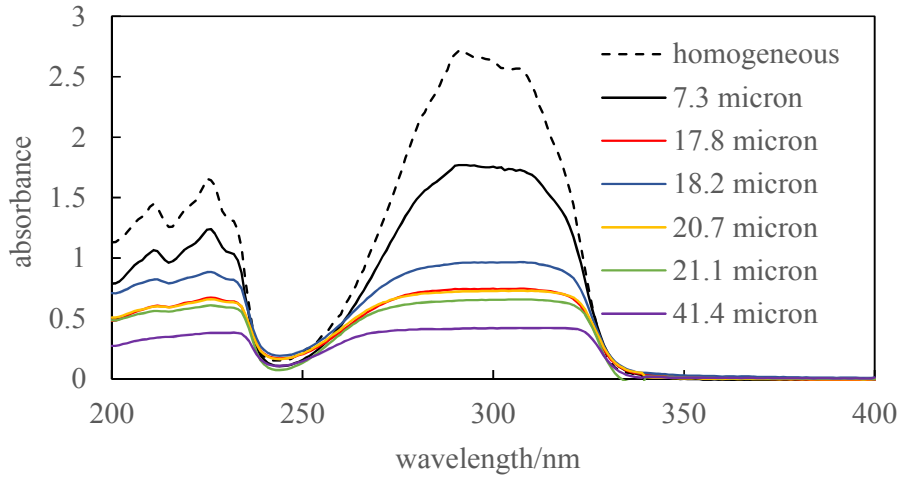

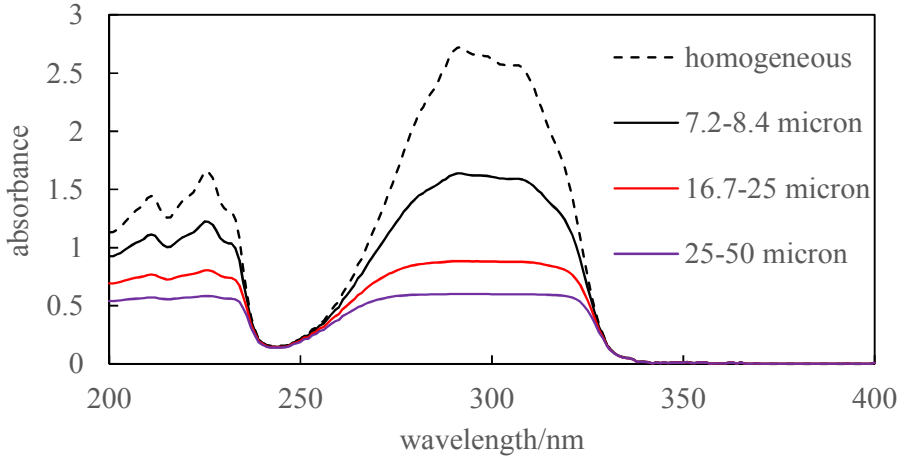

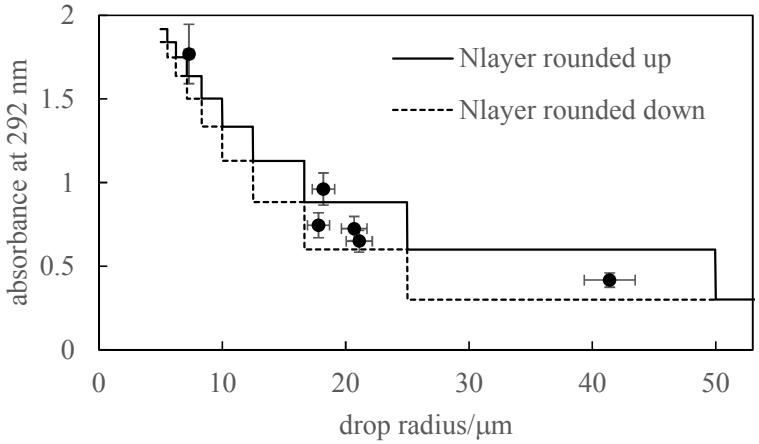

Figure 4. Comparison of measured (upper plot) and calculated (lower plot) extinction coefficient spectra for 100 μm path length of squalane-in-water emulsions with $\phi = 0.5$, mean drop radii = 15 μm and varying $[MC]_{ov}$ (shown in legend). The absorbance spectrum of the same emulsion without MC has been subtracted from each measured absorbance spectrum prior to derivation of the apparent extinction coefficient spectrum.

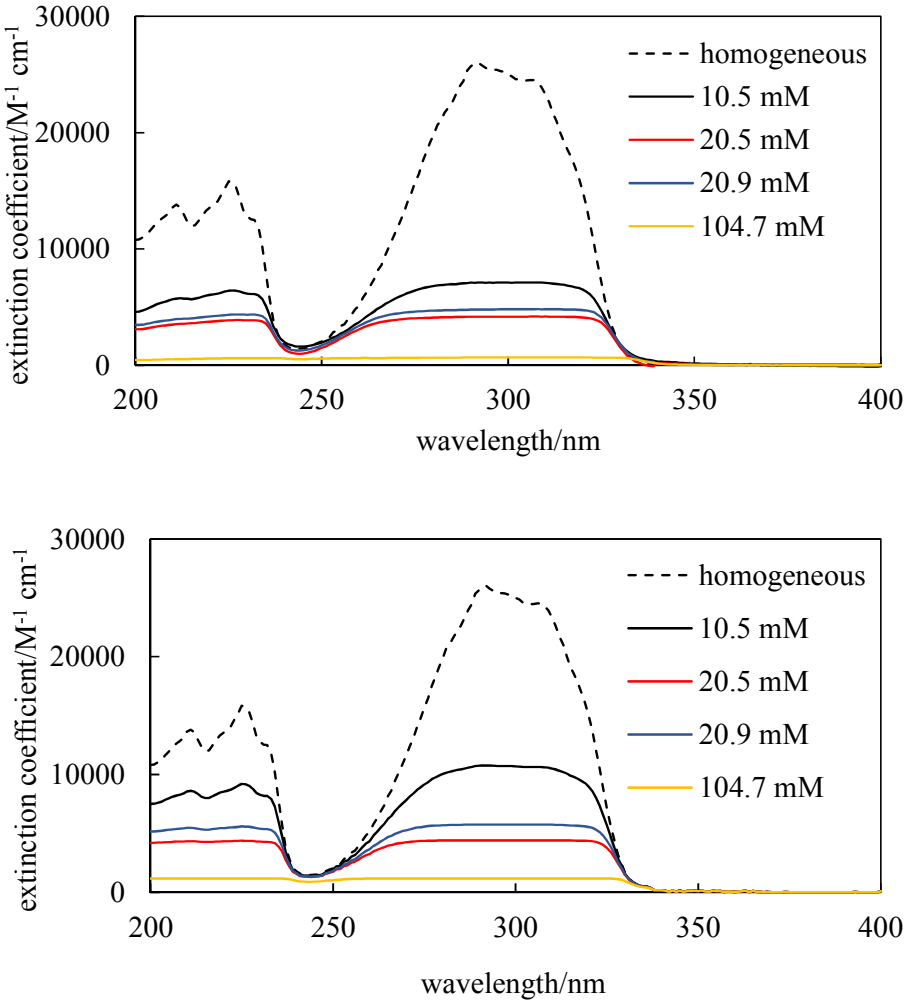

Figure 5. Comparison of measured (upper plot) and calculated (middle plot) absorbance spectra for 100 μm path length of squalane-in-water emulsions with mean drop radii = 5.8 μm, $[MC]_{SQ}$ = 10.45 mM and varying values of ϕ and $[MC]_{ov}$ (shown in legend). The absorbance spectrum of the same emulsion without MC has been subtracted from each measured absorbance spectrum. The lower plot compares measured (points) and calculated (line) peak absorbance values at 292 nm as a function of droplet volume fraction.

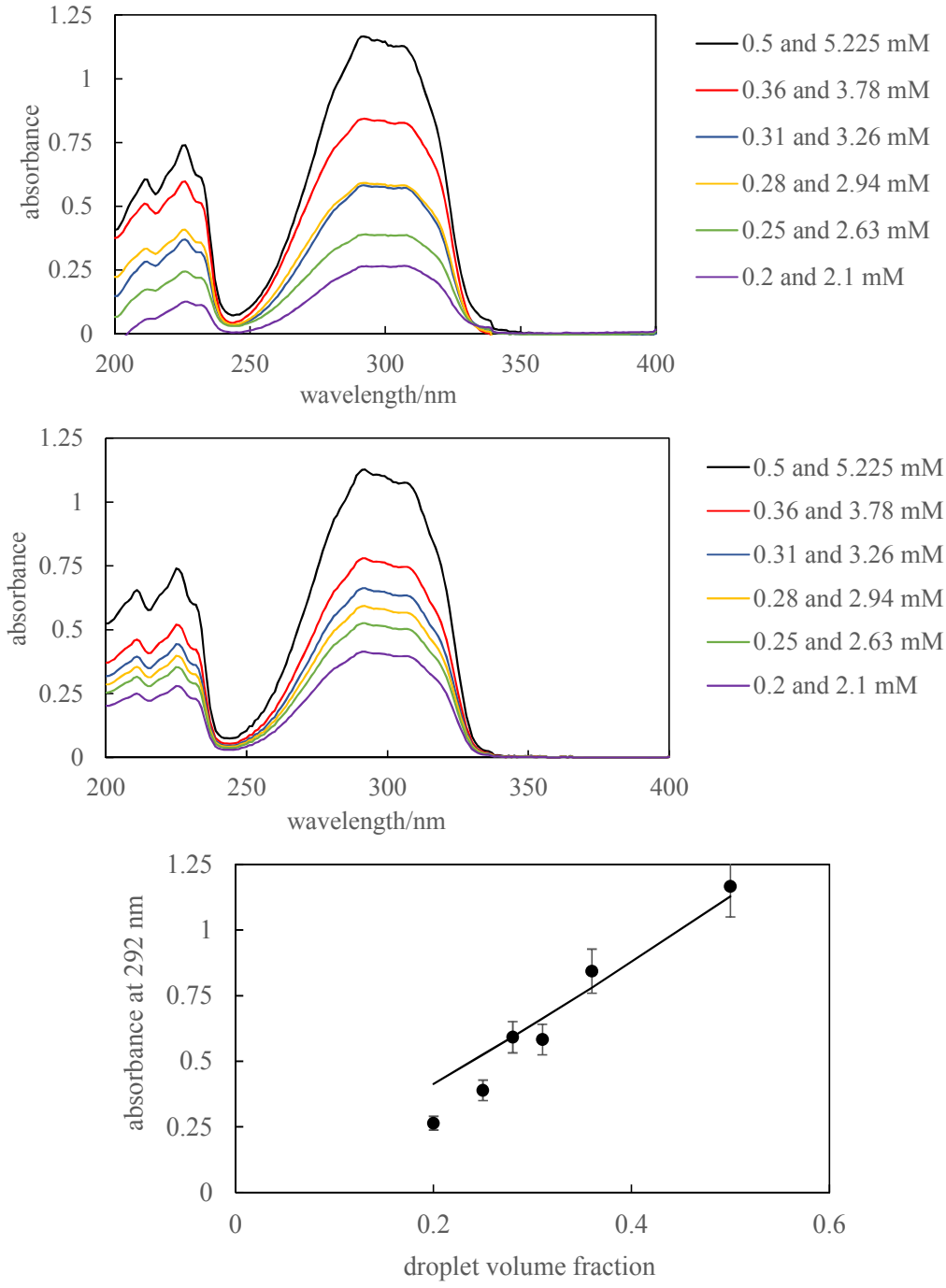

Figure 6. Comparison of measured and calculated spectra of MC in RI-matched squalane-in-sucrose + water emulsions with $\phi = 0.5$, $[MV]_{ov} = 5.23$ mM and varying mean droplet radii and path lengths (shown in the legends of the individual plots).

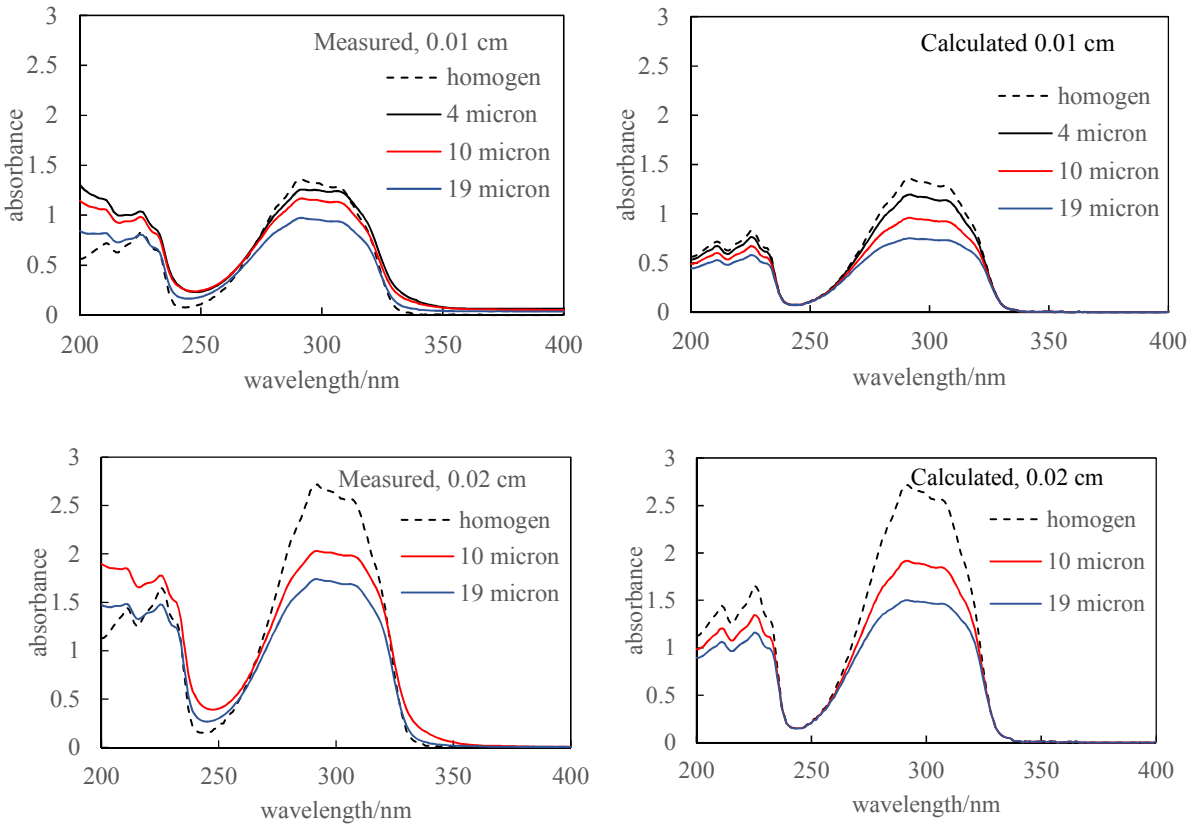

Figure 7. Model predictions of the effects of varying solute (droplet/continuous phase) distribution coefficient D for MC in PG-in-squalane emulsion films of different ϕ with path length = 0.01 cm, $[MC]_{ov}$ = 8.38 mM and r = 10 μm.

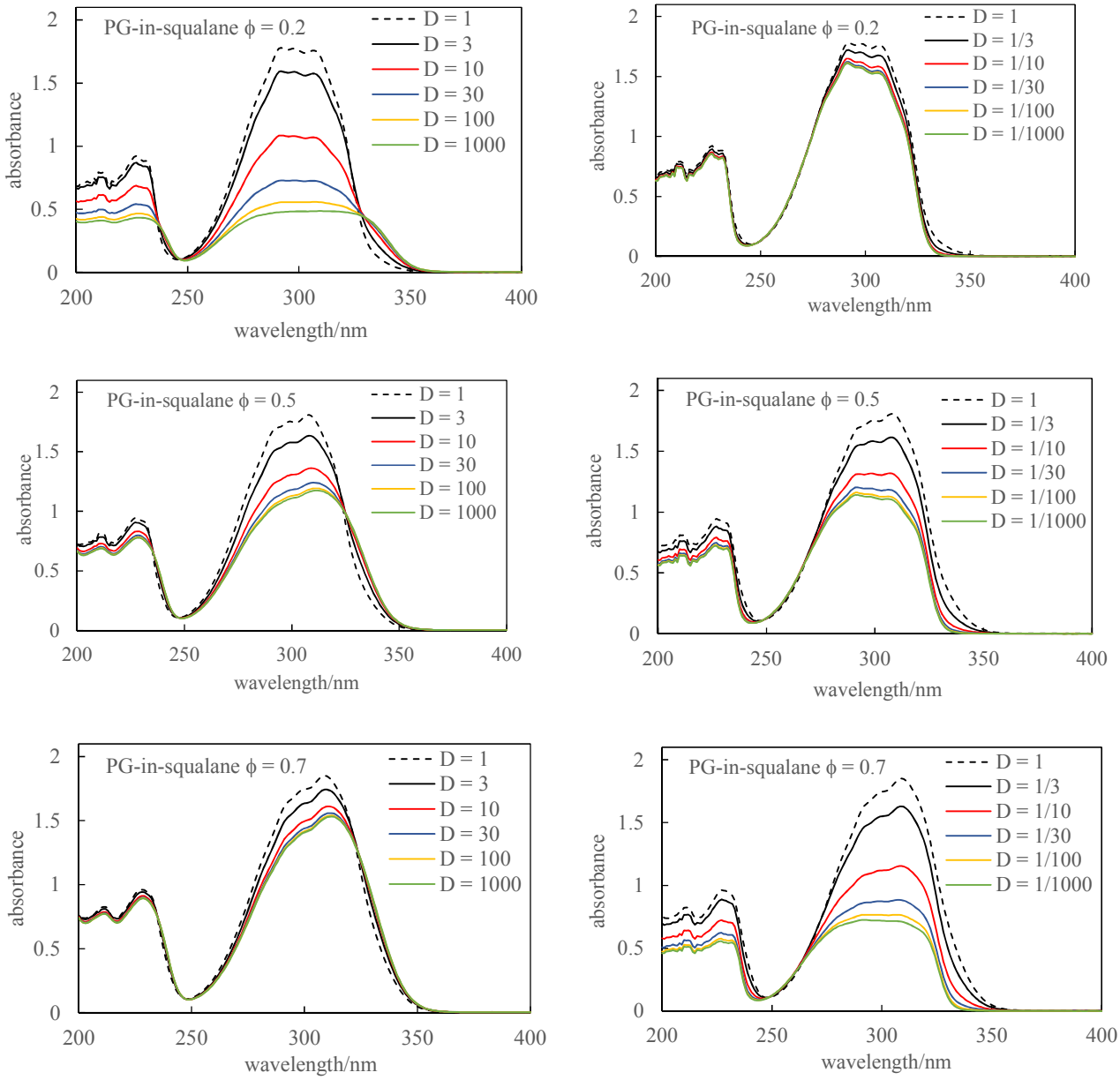

Figure 8. Comparison of measured and calculated absorbance spectra for different emulsion types. The upper plot shows MC in squalane+water emulsions; the middle plot shows AVB in squalane+PG emulsions and the lower plot shows MC in squalane+PG emulsions.

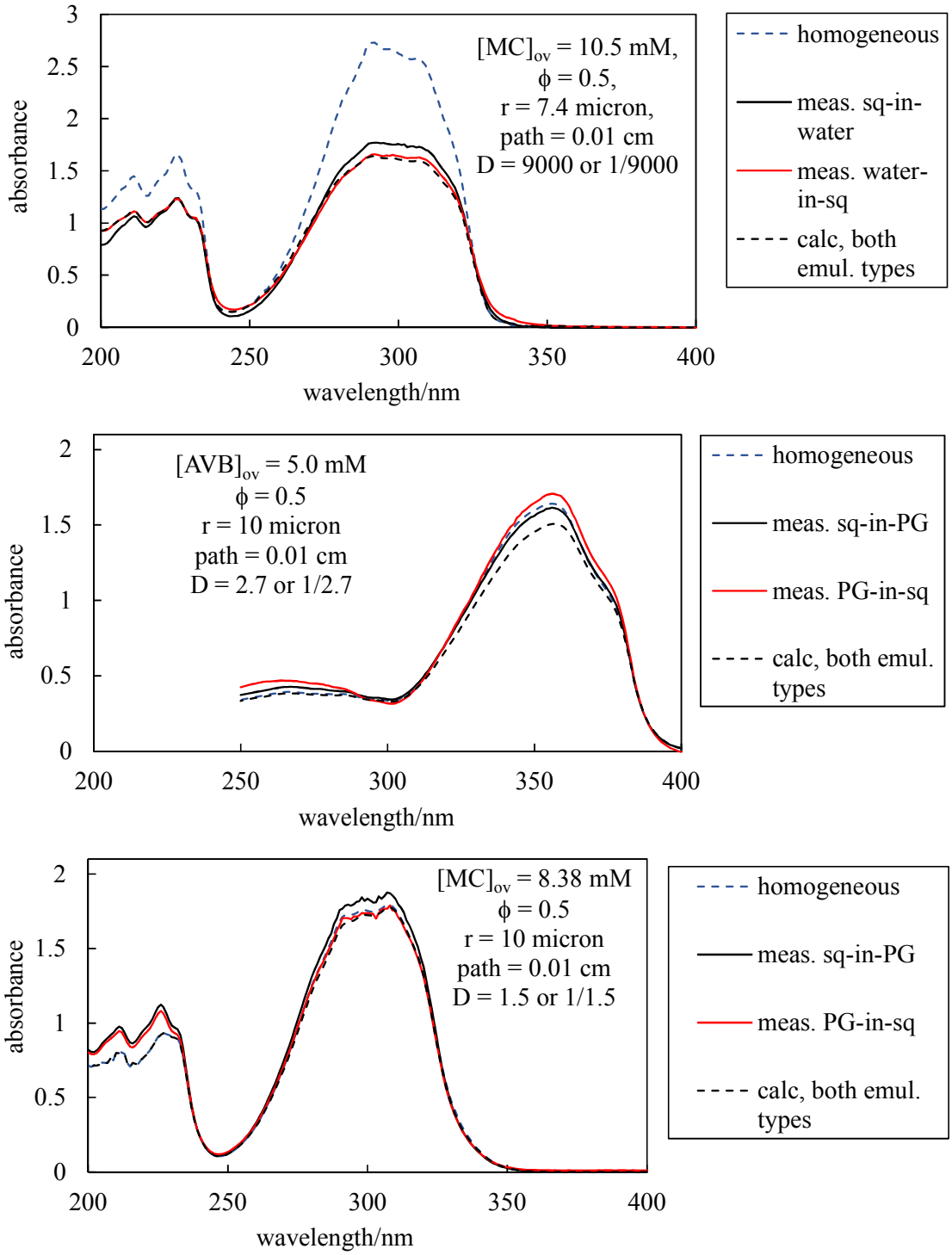

Table of Contents entry

The UV/vis absorbance spectra of coloured particle dispersions are measured and modelled.